Biosensors and Bioelectronics 142 (2019) 111595

Contents lists available at ScienceDirect

Biosensors and Bioelectronics

journal homepage: www.elsevier.com/locate/bios

An efficient disposable and flexible electrochemical sensor based on a novel and stable metal carbon composite derived from cocoon silk

Aniruddha Balkrishna Patil[a,b,*], Yafen Huang[a], Liyun Ma[a], Ronghui Wu[a,c], Zhaohui Meng[a], Lingqing Kong[a], Yifan Zhang[a,c], Wenli Zhang[a], Qiang Liu[a], Xiang Yang Liu[a,c,**]

[a] Research Institute for Soft Matter and Biomimetics, Fujian Provincial Key Laboratory for Soft Functional Materials Research, Department of Physics, College of Materials, Xiamen University, Xiamen, 361005, China
[b] Department of Chemistry, M. D. College, Parel, Mumbai, 400012, India
[c] Department of Physics, National University of Singapore, 2 Science Drive 3, 117542, Singapore, Singapore

ARTICLE INFO

Keywords:
Gold nanoparticle
Nitrogen doped silk carbon
In situ reduction
Electrochemical sensor
Rutin detection

ABSTRACT

The present work reports cocoon silk fibroin (SF)as a unique precursor for the *in-situ* fabrication of well-engineered, stable and leach free gold nanoparticle doped carbonaceous materials (AuNPs@NSC). In principle, at the molecular level, SF has a singular structure that can be converted to a N-doped aromatic carbon structure by heat treatment. The electrochemical properties of the prepared nanocomposite were examined by cyclic voltammetry and differential pulse voltammetry. A flexible three electrode sensor system with AuNPs@NSC-modified working electrodes has been developed, to achieve easy operation and quick and accurate responses. The electrochemical results showed that the sensor made by the AuNPs@NSC-modified working electrode demonstrated high sensitivity for the detection of rutin, which is attributed to the good distribution of the AuNPs on the carbon matrix. Using differential pulse voltammetry (DPV), the AuNPs@NSC electrode was found to have a linear response in the range of 0.11–250 μM and a comparably low limit of detection of 0.02 μM (S/N = 3). To ensure the accuracy and applicability of the sensors, the concentration of rutin in the commodity (rutin capsule, 10 mg/capsule) was examined, and the sensor provided high precision with a minimum relative error (RE) of 3.3%. These findings suggest that AuNPs@NSC can be considered to be a potential electrode material for the development of electrochemical devices and has great potential in extending their application to the flexible sensor field.

1. Introduction

Since the last century, silk fibroin based materials have undergone remarkable development in modern science and technology (Omenetto and Kaplan 2010). Silk fibroin (SF) materials are an interesting and abundant biomaterial with good mechanical, optical and electrical properties that are conducive to the development of next-generation biocompatible electronic devices (Hou et al. 2019; Hu et al. 2019; Tao et al. 2012; Zhu et al. 2016). SF materials are capable of achieving different forms (fiber, film, sponges, gels), which widens its application in bio-integrated conformal and biodegradable devices (Koh et al. 2015). The latest studies have shown that additional functionality of silk fibroin can be achieved by adding certain functional components to their mesoscopic network structure (Lin et al. 2016). In addition, due to the high nitrogen content, silk is considered to be the best precursor for the carbon source of N-doped carbon materials (Wang et al. 2017a).

Because of N doping and the extra-surface area, N-doped carbon materials exhibit good electrical conductivity, high mechanical strength and stable electrochemical performance and, thus, have been successfully used in the field of electrochemistry as excellent electrochemical sensors (Yang and Zhou 2017). It is well known that gold nanoparticles (AuNP) in the noble metal nanoparticle group are used to prepare electrochemical sensors (Omidfar et al. 2013). Due to their high electrical conductivity and convincing electrocatalytic performance, AuNPs can be used as a label or modifier in the sensing process, which offers additional benefits such as enhanced electric conductivity, biocompatibility and partial electrocatalytic performance (Wang et al. 2017b). The recombination of gold nanoparticles in N-doped carbon matrix

* Corresponding author. Research Institute for Soft Matter and Biomimetics, Fujian Provincial Key Laboratory for Soft Functional Materials Research, Department of Physics, College of Materials, Xiamen University, Xiamen, 361005, China.
** Corresponding author. Department of Physics, National University of Singapore, 2 Science Drive 3, 117542, Singapore, Singapore.
E-mail addresses: aniruddhapatil135@gmail.com (A.B. Patil), phyliuxy@nus.edu.sg (X.Y. Liu).

https://doi.org/10.1016/j.bios.2019.111595
Received 21 June 2019; Received in revised form 9 August 2019; Accepted 12 August 2019
Available online 12 August 2019
0956-5663/ © 2019 Elsevier B.V. All rights reserved.

materials will provide a good substrate for electrocatalysis and electrochemical sensing (Abdelhamid et al. 2017).

Rutin (vitamin P), a biologically active flavonoid glycoside, has demonstrated long range physiological functions including anti-tumor, anti-inflammatory and anti-oxidant activities (Gullón et al. 2017). As rutin has received extensive attention due to its pharmaceutical and clinical applications, it is essential to know the exact level of rutin. In this regards, several new and sensitive methods for rutin analysis have been developed, such as spectrophotometry (Xu et al. 2010), chemiluminescence and electrophoresis (Liang and Song 2008), high-performance liquid chromatography (Yildirim et al. 2017), capillary and solid extraction methods (Marti et al. 2017). However, these methods suffer from various limitations, such as the complexity of the instrument, high cost, time-consuming operation, poor sensitivity and usage of hazardous chemicals. Consequently, it is important to identify reliable and accurate rutin analysis methods that are sensitive, low-cost and simple. The presence of electroactive flavonoid glycoside groups in the molecular structure of rutin generates electrochemical responses; therefore, electrochemical methods have been explored as the preferred method for measuring rutin concentrations. For instance, a variety of materials have been explored as an electrode for electrochemical analysis of rutin. Niu et al. prepared a composite of graphene and gold nanoparticle nanoparticles for rutin detection (Niu et al. 2018a); Liu et al. has prepared graphene-palladium nanoparticles for rutin detection (Liu et al. 2017). Yang et al. designed N-doped graphene supported gold-silver nanothorns as a sensitive material for the chemical detection of rutin (Yang et al. 2018). However, all of the above electrode materials include *ex situ* operations, in which metal nanoparticles are doped on the surface of the conductive support. Such an electrode material faces a major problem of catalyst leaching. In this regard, the development of stable, sensitive and selective electrode materials, that will provide accurate, reproducible and reliable results is in high demand; however, at the same time, the development of such methods is also a challenge.

In the present work, we establish a new composite material, i.e., AuNPs@NSC using cocoon silk chemistry via an *in situ* synthesis protocol for the detection of rutin. A simple, cost effective and environmentally friendly *in situ* synthesis strategy was used to fabricate well-dispersed gold nanoparticles (AuNPs) in the host of porous and conductive carbon matrix prepared *in situ*. The product obtained has a high content of nitrogen and well-distributed AuNP in the carbon matrix, facilitating rapid charge transfer, additional charge capacity, ease of electrolyte interaction and optimum mass transfer. The host AuNPs provide a rich active site, while the NSC matrix, in addition to providing improved conductivity serve as a protective cage, which could improve the stability of AuNPs in catalytic and electrocatalytic applications. Furthermore, a flexible strip based three electrode sensor system with the AuNPs@NSC-modified working electrodes was developed. The prepared AuNPs@NSC-modified sensor system achieved easy operation and quick and accurate responses with high stability and sensitivity for the detection of rutin levels. The sensor exhibited high accuracy in the estimation of a commercial rutin product (rutin capsule). Furthermore, the strategy demonstrated an efficient and general route for a leach free catalytic system, providing opportunities for a heterogeneous catalysis process.

2. Experimental

Details about the chemicals, AuNPs@NSC preparation and material characterization are discussed in the supporting information S1 to S5.

2.1. Electrochemical measurements of rutin

All of the electrochemical measurements were performed using an electrochemical station CHI66. The three-electrode flexible strip-based sensor system was developed, which includes a platinum counter electrode (CE), an Ag/AgCl reference electrode (RE) and a working electrode (WE) modified with AuNPs@NSC (Fig. 2).

2.2. AuNPs modified three electrode sensor

In a typical fabrication protocol, a three-electrode sensor pattern is first designed using adobe illustrator (AI) software, then a paper mask with the desired pattern is prepared by laser cutting according to the AI design and attached to polyethylene terephthalate (PET) film. The film is then subjected to magnetic sputtering to obtain a platinum conducting pattern. Finally, the patterned electrode with a platinum conducting network is obtained by peeling off the paper mask. Except for the working area and the connection points, the rest of the parts of the conductive track are covered by insulation film to avoid cross connections.

Accurately weighted 5.0 mg of AuNPs@NSC is added to 1 mL of DI water containing 0.05% (w/v) of Nafion® as a binder. The above mixture is exposed to ultrasonication for 10 min at room temperature to produce a homogeneous suspension. A volume of 10 µL of the aqueous dispersion is deposited on the working area and dried at 60 °C under vacuum for 1 h. The solid Ag/AgCl reference electrode was prepared by drop casting 20 µl (10 mg/ml) of the AgNWs aqueous solution on the reference electrode area, which was then chlorinated using 0.1 M $FeCl_3$, followed by annellation at 80 °C for 15 min. The third electrode i.e. counter electrode is platinum.

3. Results and discussions

Fig. 1 is a schematic illustration of the proposed synthesis method, in which AuNPs are prepared *in situ* and hosted into an *in situ* prepared nitrogen-doped carbon matrix (NPC) using cocoon silk as a carbon precursor. In principle, under high temperature treatment, the adjacent amide bonded protein chains of RSF can transform to aligned polyaromatic carbon structures due to intermolecular dehydration (Fig. 1A) (Hou et al. 2015). In a typical synthesis protocol, the RSF solution is initially prepared using raw *Bombyx mori* silk cocoons (Fig. 1B). In second step AuNPs are fabricated by a BSA molecule in alkaline pH condition (10–12) (the BSA molecule has high reduction ability in alkaline medium (Xie et al. 2009) (Fig. 1C). In the fabrication of AuNPs, BSA plays a key role in the reduction and encapsulation process (Xie et al. 2009). Here, the selection of BSA is based on two principal reasons, one reason is the availability of mercapto groups (-SH) that reduce Au (III) into Au (0) then to gold nanocluster (AuNCs) and finally to AuNPs, which are further encapsulated and stabilized by the BSA protein molecules. The other reason is BSA can be easily mixed with the RSF solution due to common amino groups (Tu et al. 2016). In a subsequent step, the prepared bioconjugates are subjected to freeze drying where water-based (or solvent based) suspensions are transformed to a solid mass. The formation and encapsulation of AuNPs by protein molecules were investigated by Fourier transform infrared spectroscopy (FTIR) (Fig. S1). A wagging end-gauche defect band at 1083 cm^{-1} was observed, which is an important characteristic feature of the Au–S clusters (Gaur et al. 2012). In general the Au–S vibration peaks are very weak and difficult to notice, although there have been reports on FTIR investigations of Au–S clusters (Petroski et al. 2009). The solid mass is then pyrolyzed under a nitrogen atmosphere to achieve a well-ordered carbon structure with improved electrical conductivity. The pyrolysis technique limits the diffusion and migration of the as-obtained Au nanoparticles and enables a uniform NP distribution across the bulk of NPC. The obtained AuNPs@NSC product showed considerably improved electrochemical properties in comparison to that of the product without gold carbon and bare carbon electrodes. In generally, chemical activation followed by carbonization method has been extensively used to target AuNPs@NSC as a good conductive material. Here, during the carbonization process, the available AuNPs in the composite mass show a catalytic effect and elevate the evolution of volatile components creating numerous abundant pores (Zhu et al. 2018). Therefore, the

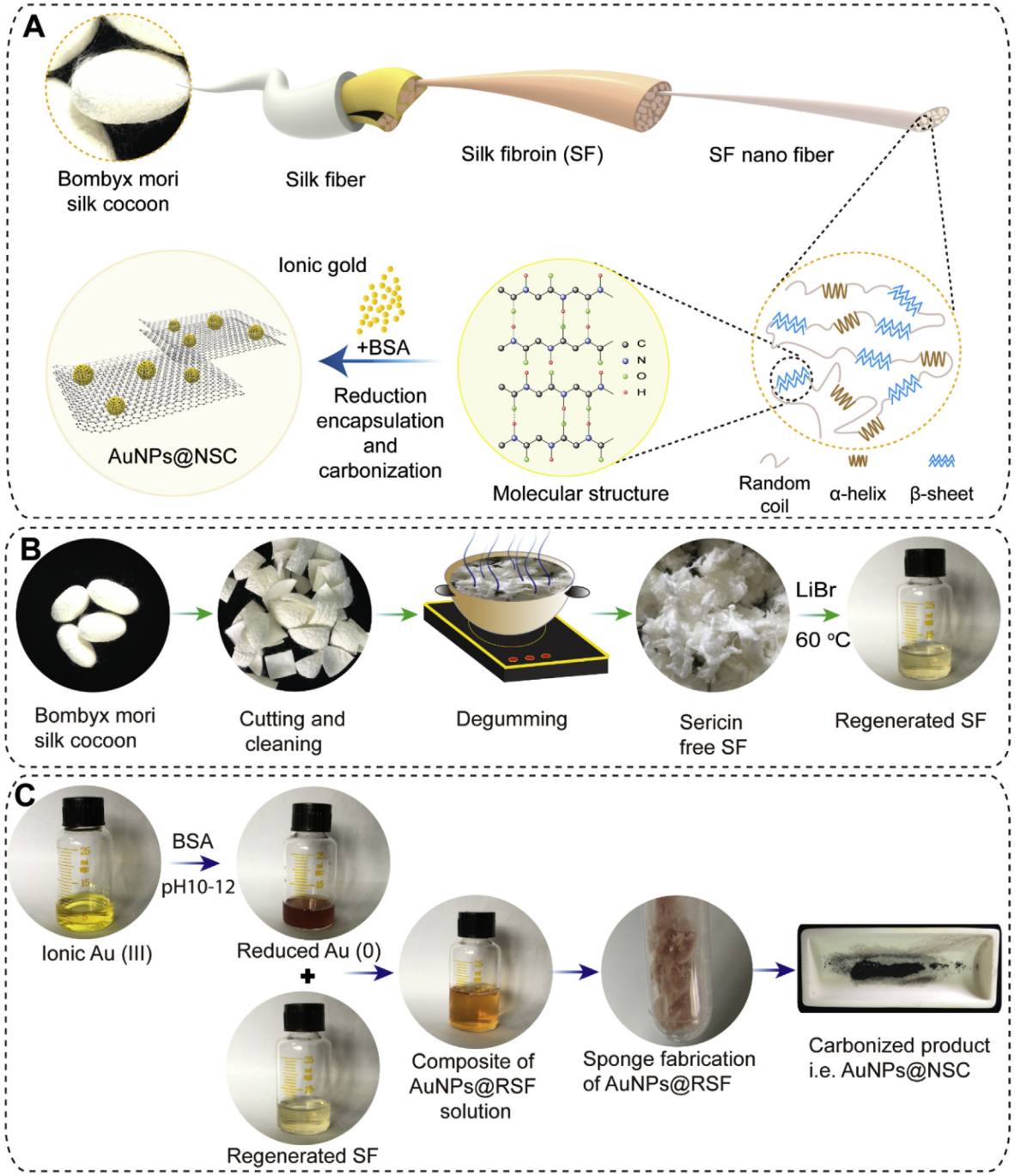

Fig. 1. Schematic illustration of the AuNPs@NSC composite material preparation. (A) Schematic illustration of the multistage structure of the silk protein and AuNPs@NSC composite material. (B) Systematic illustration showing the preparation of regenerated silk fibroin (RSF) from cocoon silk. (C) Schematic illustration showing the *in situ* reduction of AuNPs using bovine serum albumin (BSA) molecules, the preparation of AuNPs@BSA + RSF composite, the formation of AuNPs@BSA + RSF sponge, and the final carbonized AuNPs@NSC composite material.

existence of AuNPs in the synthesis has a decisive effect on the carbon texture.

3.1. Characterization of AuNPs@NSC

SEM and TEM analyses were performed to evaluate the morphology of the prepared composite and the degree of the dispersion of the AuNP on the NSC. The SEM images of AuNPs@NSC (Fig. 3A and B) show a large number of uniform, well-distributed, homogeneous, spherical and non-agglomerated dispersions of gold nanoparticles hosted in the nitrogen-doped porous carbon matrix. Based on the TEM images of AuNPs@NSC (Fig. 3C and D), the prepared AuNPs are spherical in size and well dispersed on the carbon matrix, corroborating the SEM results. A large number of AuNPs were formed in the carbon matrix, and the average size of the Au nanoparticles was ~25 nm, demonstrating the temporal confinement carbonization conditions on the synthesis of ultrafine NPs. The amount and distribution of AuNPs in the composite mass is a key factor for electrochemical applications; therefore, the optimum mixing ratio of AuNPs@BSA with RSF was investigated, and three different concentrations of AuNPs@BSA:RSF were studied, i.e., 40:60%; 50:50% and 60:40%. Fig. S2 shows the TEM images with particle size distributions of the carbonized mass with these

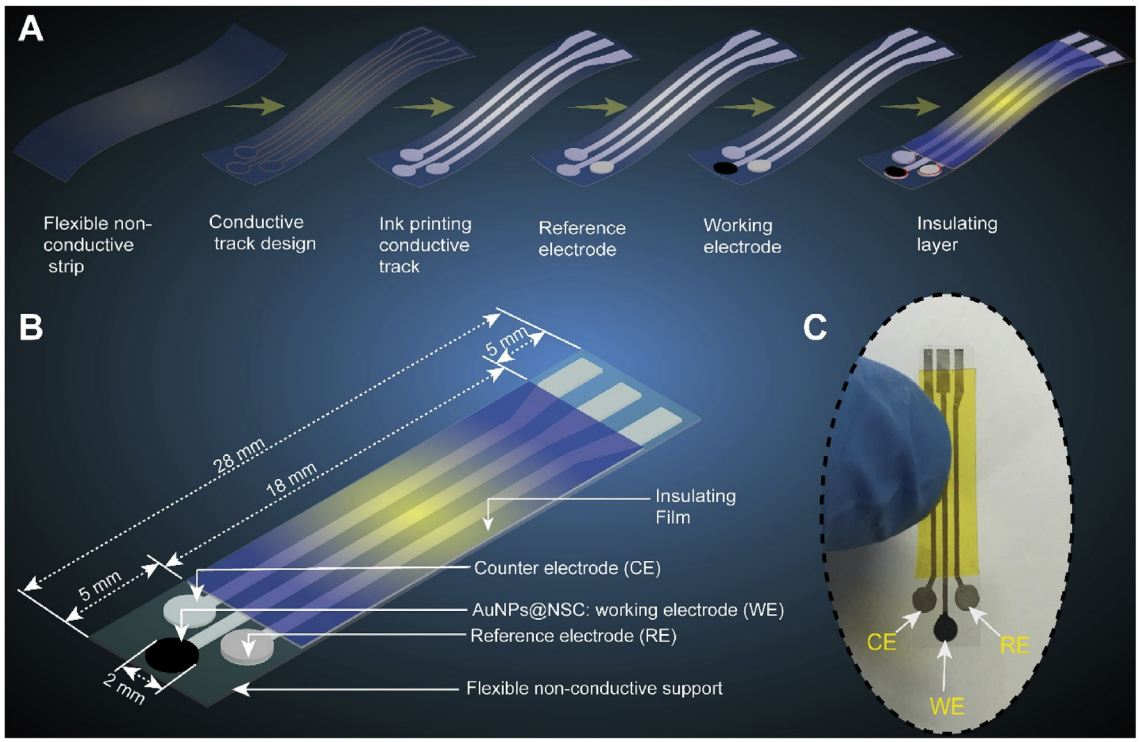

Fig. 2. Three-electrode AuNPs@NSC-modified flexible strip sensor. (A) Schematic representation of the fabrication process. (B) Dimensions. (C) Actual photograph of the three-electrode flexible strip-based sensor.

concentrations. By altering the ratio, the average nanoparticle size and distribution change dramatically, where the addition of 40% and 50% AuNPs@BSA leads to spherical morphology with narrow size distribution (25 ± 10 nm). In contrast, at 60% AuNPs@BSA, randomly distributed, disordered AuNPs were obtained because at excessive concentration, AuNPs can easily aggregate during carbonization. These results indicate that material formed with the 50:50% AuNPs@BSA:RSF concentration possesses homogeneous, well distributed and high percentage AuNPs. Therefore, these AuNPs are the best for electrocatalytic performance. The XRD patterns of the NSC and AuNPs@NSC nanocomposites are recorded in the 2θ range of 10–90°, and the results are presented in Fig. 3E. In the XRD pattern, a broad graphitic peak is observed at approximately 25.3°, which belongs to the crystal graphite plane (002) of NSC. The XRD pattern of AuNPs exhibited five peaks at 37.8°, 44.1°, 64.5°, 77.3° and 81.8° indexed to the (111), (200), (220), (311) and (222) planes of Au nanoparticles, respectively. In comparison with the pattern of bulk Au from the Joint Committee on Powder Diffraction Standards (JCPDS:65–2870), the diffraction peaks from the synthesized Au nanoparticles are located at the same angles, confirming their formation.

There are two intense peaks at 1340 cm^{-1} (D-band) and 1590 cm^{-1} (G-band) in the Raman spectrum (Fig. 3F). A D-band corresponds to the amorphous or disordered structure of the AuNPs@NSC, while the G-band corresponds to the C–C symmetric stretching. The I_D/I_G ratio was used to calculate the degree of structural disorder (e.g., defects on surface, vacancies, kinks and heteroatoms). The I_D/I_G ratio was greater in the AuNPs@NSC(1.02) than in the NSC (0.99), which is due to the increase in structural defects on the AuNPs@NSC surface as a result of the insertion of AuNPs in the graphitic structure.

XPS measurement was used to investigate the elemental compositions and states of the as-prepared AuNPs@NSC (Fig. 4). The survey spectra exhibited four obvious peaks at 93.24 (Au 4f), 285.37 (C 1s), 409.24 (N 1s) and 532.26 (O 1s), confirming the presence of the C, O, N and Au elements (Fig. 4A). The C 1s spectrum of AuNPs@NSC (Fig. 4B) was rationally deconvoluted into five types of carbon located at 284.5 eV (C═C bonds), 285.1 eV (C–C bonds), 286.3 eV (C–O bonds), 287.3 eV (C–N bonds) and 289.2 eV (O–C═O bonds). The O 1s spectrum (Fig. 4C) was fitted into three peaks: C–O, C═O and O–C═O at the respective binding energy of 531.4 eV, 532.6 eV, and 533.5 eV. The N 1s peak appeared at approximately 400.0 eV, indicating successful doping of N into the carbon matrix, which further deconvoluted into four peaks assigned to pyridine N (398.5), pyrrolic N (399.8), quaternary N (401.3) and N-oxide (402.7) (Fig. 4D). Fig. 4E shows the high-resolution spectra of Au 4f, two intense peaks at binding energies of 84.2 eV and 87.8 eV were recorded, corresponding to Au $4f_{7/2}$ and $4f_{5/2}$, respectively. These peaks indicate that Au are in a distinct metallic state in AuNPs@NSC.

3.2. Electrocatalytic activity on the different-modified electrodes

The electrocatalytic performance of prepared electrode AuNPs@NSC were estimated by cyclic voltammetry (CV). The cyclic voltammograms obtained at a scan rate of 100 mV/s of bare carbon, NSC, and AuNPs@NSC electrodes in 0.1 M PBS (pH = 4.0) containing 0.1 mM rutin are shown in Fig. 5A. The oxidation and reduction peaks were observed in a 0.1 mM rutin solution, which demonstrate a two-proton two-electron electrochemical reaction of rutin on the electrode support (Yang et al. 2017). The acquired results show that AuNPs@NSC has the strongest electrocatalytic activity for rutin sensing compared with NSC and carbon. Scheme 1 shows the redox reaction of rutin possessing hydroxyl groups and the oxidation of dihydroxyl groups on the surface of AuNPs@NSC electrode. Fig. 5B shows the CV plots of the AuNPs@NSC electrode with or without 0.1 mM rutin in 0.1 M PBS (pH = 4.0). A significant redox peak was obtained for 0.1 mM rutin in 0.1 M PBS (pH = 4.0) that was attributed to the redox activity of rutin on the AuNPs@NSC surface.

3.3. Influence of buffer pH

The performances of the AuNPs@NSC electrode in the detection of

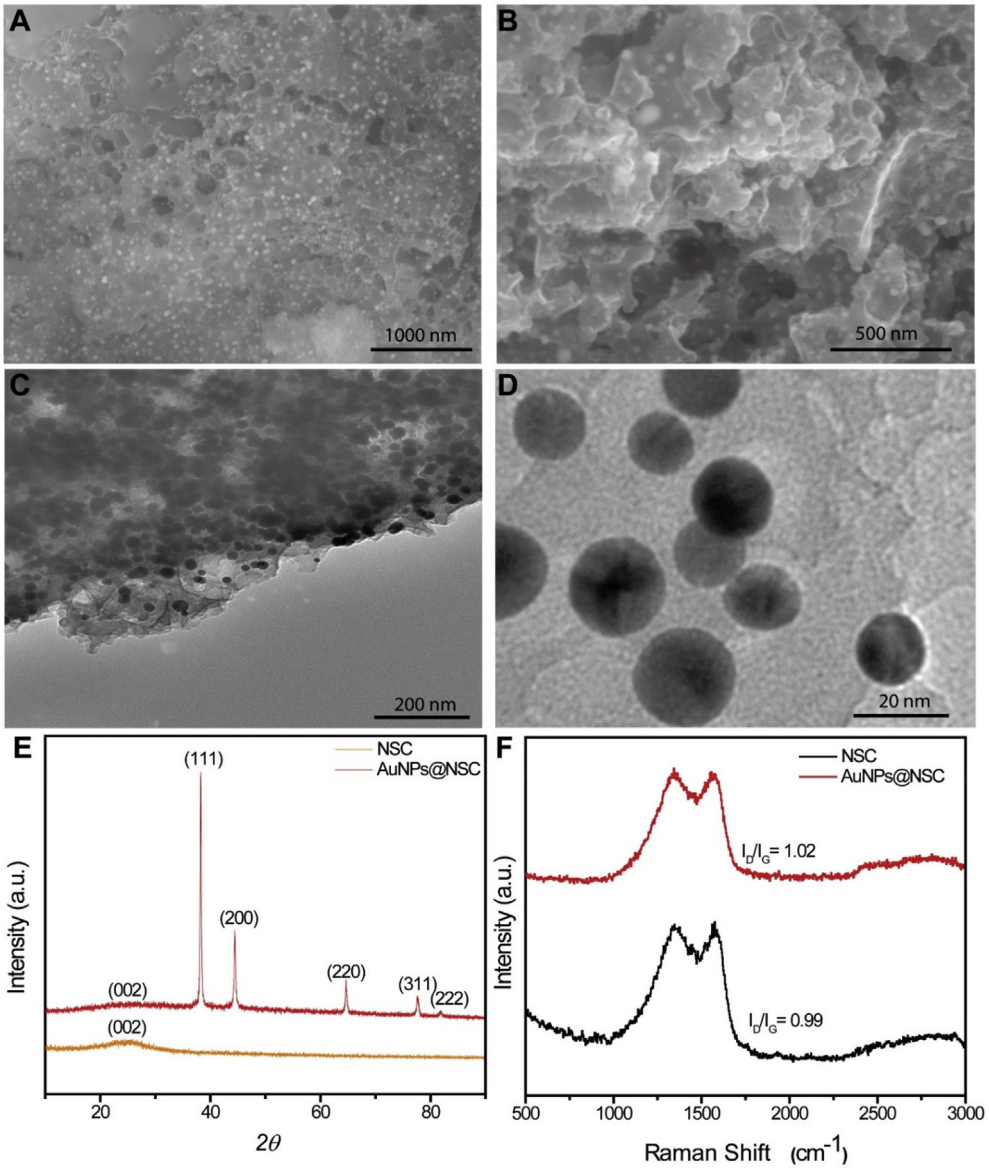

Fig. 3. Structural characterization of the as-prepared AuNPs@NSC. (A and B) SEM images of the AuNPs@NSC with different magnification. (C and D) TEM images of the AuNPs@NSC with different magnification. (E) XRD spectra of the NSC and AuNPs@NSC. (F) Raman analysis spectra of the NSC and AuNPs@NSC.

the rutin concentration were evaluated with a series of buffer pH solutions under the optimized experimental setup. Fig. 5C and D shows the CVs of the 0.1 M PBS solutions containing 0.1 mM rutin with a pH ranging from 3.0 to 6.0. In all cases, a pair of well-defined redox peaks were observed with a change in the electrochemical response, with a shift of the redox peak potentials towards lower potential value with an increase in buffer pH that determines the involvement of protons in the electrochemical reaction. Furthermore, as shown in Fig. 5D, the maximum value of I_{pa} appeared at a pH of 4.0 and subsequently decreased with a further increase in the pH, providing the appropriate evidence for the selection of the optimal pH for the analytical detection of rutin.

3.4. Influence of scan rate

The effect of the scan rate on the 0.1 mM rutin solution in 0.1 M PBS (pH = 4.0) at the AuNPs@NSC electrode was studied. The obtained results showed gradual increment in both cathodic and anodic peak currents with as the scan rate changed from 20 mV/s to 200 mV/s (Fig. 5E). A good linear relationship between the redox peak currents (I_p) and the scan rate (υ) was observed (Fig. 5F). Two regression equations were developed using the oxidation and reduction peak current values, I_{pa} (μA) = 0.4245 x υ (mV/s) - 5.0865 (R^2 = 0.9953) and I_{pc} (μA) = −0.4118 x υ (mV/s) + 4.3819 (R^2 = 0.9957), demonstrating that the electrochemical redox reaction of rutin on the AuNPs@NSC electrode surface is an adsorption controlled reaction (Niu et al. 2018a). Alternatively, the shift in the redox peak potentials with the increase of the scan rate (Fig. 5G) demonstrates a quasi-reversible electrochemical reaction. The redox peak potential on ln υ obeyed the linear regression equations as E_{pa} (V) = 0.027 ln υ + 0.1232 (R^2 = 0.9633) and E_{pc} (V) = −0.022 ln υ + 0.2501 (R^2 = 0.9584). The number of electrons involved in the reaction was calculated using Laviron's equation, in which 'α' is defined as the charge transfer coefficient, and 'n' is number of electrons.

$$E_{pa} = E'^{0} + \frac{RT}{(1-\alpha)nF}\ln(\nu) \quad (1)$$

$$E_{pc} = E'^{0} - \frac{RT}{\alpha nF}\ln(\nu) \quad (2)$$

The redox reaction parameters are defined with slopes of linear

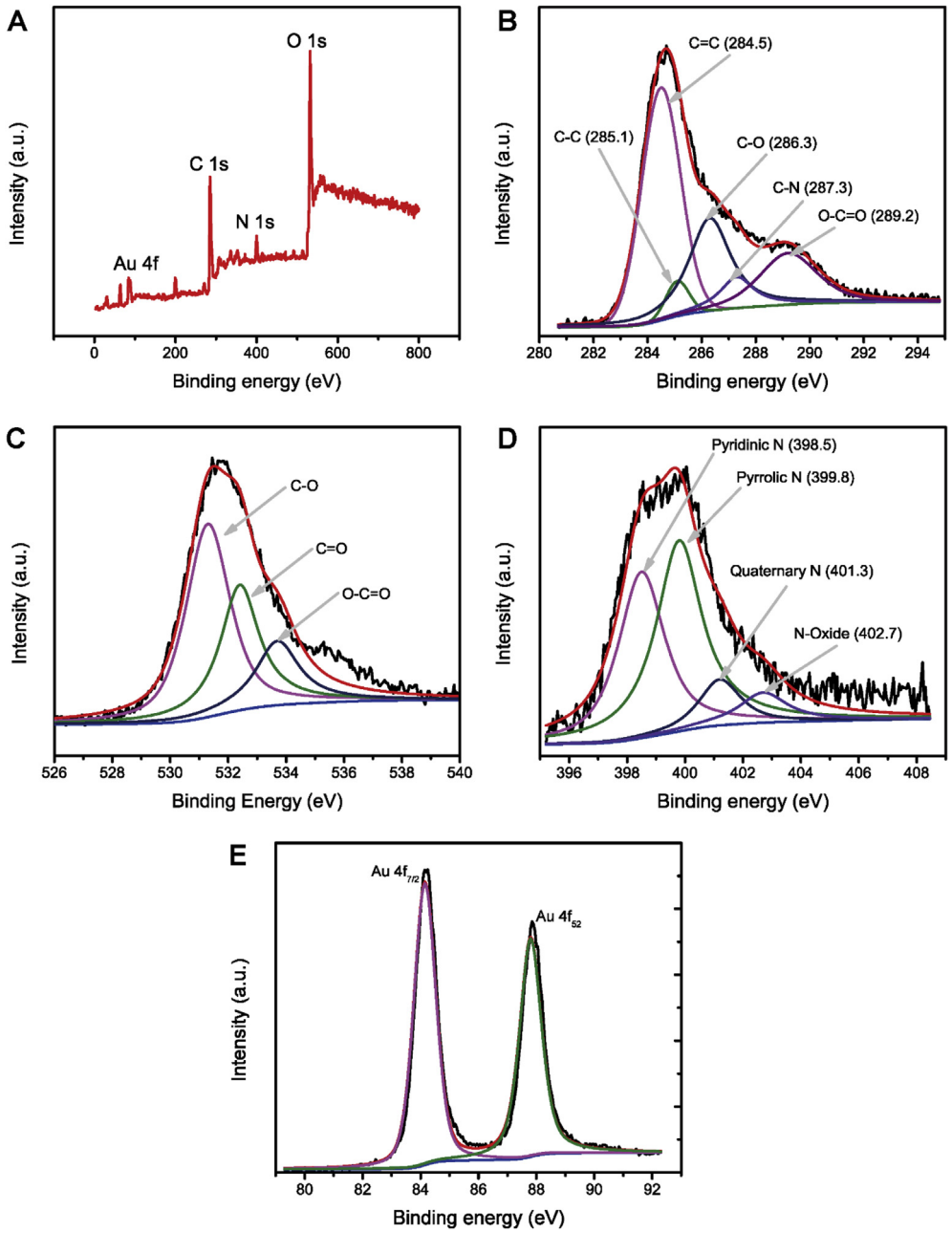

Fig. 4. XPS analysis spectra of the AuNPs@NSC composites. (A) Survey XPS of the AuNPs@NSC composites. (B) XPS core level spectra of C 1s. (C) XPS core level spectra of O 1s. (D) XPS core level spectra of N 1s. (E) XPS core level spectra of Au 4f.

plots between E_{pa} and ln ν and between E_{pc} and ln ν for RT/(1-α)nF and RT/αnF. By combining Eqs. (1) and (2), α and n were calculated as 0.5053 and 1.7460, respectively. The calculated n value of 1.746 is close to 2, which indicates the involvement of 2 electrons in the reaction of rutin, which is also consistent with previously reported results. (Yang et al. 2017, 2018; Zou et al. 2016). Hence, the electrooxidation reaction of rutin on the AuNPs@NSC exhibits a two-electron two proton mechanism.

3.5. Detection range of rutin on the AuNPs@NSC-modified electrode

Under optimal conditions, the electrochemical performance of AuNPs@NSC in rutin detection was investigated by differential pulse voltammetry (DPV) at pH = 4.0, in the potential range of 0.0 – 0.6 V (vs. Ag/AgCl). The DPV measurements were used to determine the rutin concentration due to its high sensitivity and selectivity. The obtained results are shown in Fig. 5H, in which the oxidation peak current increased with an increased concentration of rutin from 0.11 μM to 250 μM and revealed a linear relationship. Fig. 5H (inset) shows the linear fitting curve for the relation between oxidation currents and rutin concentrations. The linear regression equation was calculated as I_{pa} (μA) = 0.0674 x C(μM) + 57.43 with a correlation coefficient of 0.9969 (C = 0.11–250 μM). Based on the signal-to-noise ratio (S/N = 3), the curve reached a relatively low limit of detection of 0.02 μM with a linear range. Based on different-modified materials, a comparison of rutin detection is listed in Table 1. As shown in Table 1, the AuNPs@NSC electrode exhibited a relatively broader detection range with a lower limit of detection.

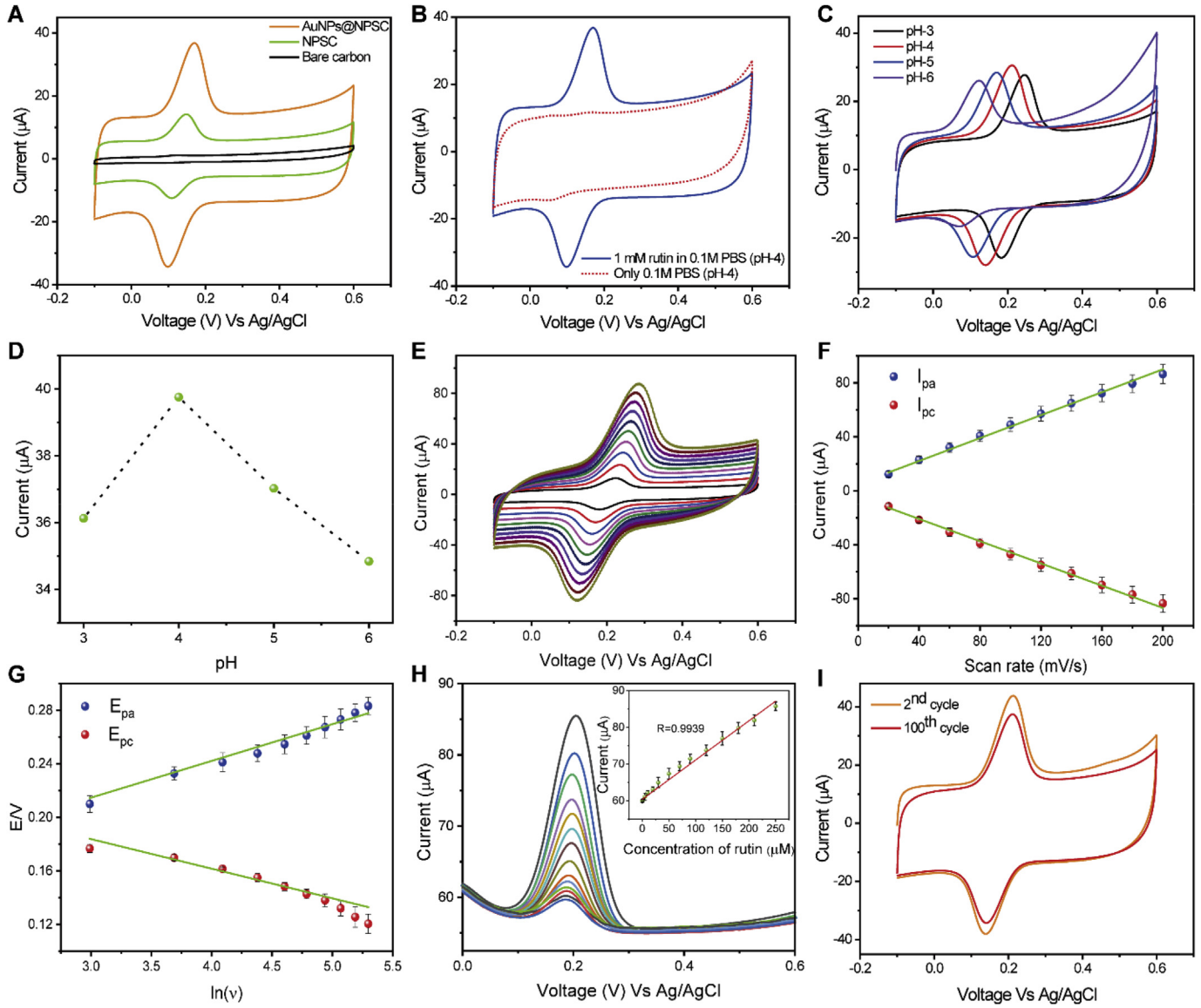

Fig. 5. Electrocatalytic performance of AuNPs@NSC. (A) CVs of AuNPs@NSC, NSC and bare carbon electrodes recorded in 0.1 M PBS (pH 4) containing 0.1 mM rutin at a scan rate of 100 mV/s (B) CVs of AuNPs@NSC, electrode recorded in 0.1 M PBS (pH 4) with and without 0.1 mM rutin at a scan rate of 100 mV/s (C) CVs of AuNPs@NSC electrode in 0.1 mM rutin at various pH PBS solutions (scan rate of 100 mV/s). (D) The relationship between the oxidation peak current (I_{pa}) and pH. (E) CV curves of the AuNPs@NSC electrode in 0.1 M PBS (pH 4.0) solution containing 0.1 mM rutin at different scan rates from 20 to 200 mV/s. (F) Graph showing anodic and cathodic peak currents versus the scan rate. (G) Graph of anodic and cathodic peak potentials versus ln ν. (H) DPV curves of AuNPs@NSC electrode in 0.1 M PBS (pH = 4) solution containing different concentrations of rutin from 0.011 to 250 μM. Insets: A curve fitting plot of oxidation peak current vs. concentration of rutin. (I) 99 cycles of the stability test in 0.1 M PBS (pH 4) containing 0.1 mM rutin.

3.6. Reproducibility and stability study of the AuNPs@NSC- modified sensor

The reproducibility of the prepared AuNPs@NSC-modified sensors was evaluated using five strip sensors, and the peak currents were recorded by DPV measurements in 0.11–250 μM rutin solutions. The relative standard deviation (RSD) of the AuNPs@NSC-modified sensor for detecting 250 μM rutin was calculated using 5 sensors; the RSD was 1.52%, indicating excellent reproducibility.

The stability of the AuNPs@NSC-modified sensors was examined by recording 100 successive CV cycles in 0.1 M PBS (pH = 4.0) containing 0.1 mM rutin solution (Fig. 5I). The oxidation current response of rutin after the 100th cycle was 89.3% of that of the 2nd cycle, revealing excellent stability of the as-prepared AuNPs@NSC-modified sensors during the oxidation process.

3.7. Influence of foreign species

Furthermore, the interference of foreign species in the detection of rutin was evaluated, in which the effect of potential interfering species, such as lactic acid, sodium lactate, D-glucose, citric acid, potassium chloride, sodium acetate, sodium diphosphate, disodium phosphate and sodium sulfate, on the detection of 1.0×10^{-6} mol/L rutin was examined; the obtained results are shown in Table S1. Except for citric acid (3.78% RE), all other species showed less than 2% RE, indicating excellent performance of the as-proposed AuNPs@NSC-modified sensor with negligible influence. The voltammetry response was nearly unchanged in the presence of the abovementioned compounds, which suggests that the detection of rutin is minimally affected by the presence of these main excipients.

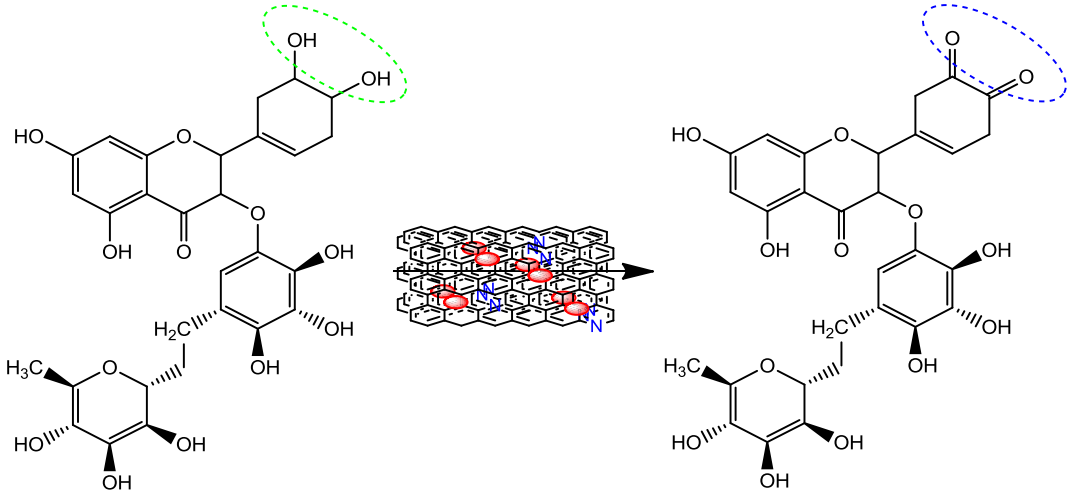

Scheme 1. Schematic representation of rutin detection on AuNPs@NSC using an electrochemical method.

Table 1
Comparison of the performance of various electrodes in rutin detection.

Electrodes	Linear range (μM)	LOD (μM)	Reference
AuNPs/en/MWNT	0.048–0.96	0.032	Yang et al. (2010)
AuNPs/GR	0.1–15	0.01	Apetrei and Apetrei (2018)
Cu/chitosan/MWCNT	0.05–100	0.01	Gholivand et al. (2016)
AuNPs/CNT	0.1–31	0.08	Yang et al. (2017)
IL-CCE	0.3–100	0.09	Zhan et al. (2010)
Fe_2O_3/RGO	0.015–18	0.001	Wu et al. (2015)
C–Cu-resin	0.9–8	0.026	Freitas et al. (2009)
Au–Ag/NG	0.05–241.2	0.01	Yu and He (2015)
BP–PEDOT:PSS/GCE	0.02–80	0.007	Niu et al. (2018b)
Mg–Al–Si@PC/GCE	1–10	0.01	Yalikun et al. (2019)
AuNPs@NSC	0.11–250	0.02	This work

en: ethylenediamine; MWNT: multiwalled nanotubes; GO: graphene oxide; IL: ionic liquid; RGO: reduced graphene oxide; PtNP: platinum nanoparticles; GR: graphene; NG: nitrogen-doped graphene; GCE: glassy carbon electrode, CCE: carbon ceramic electrode, BP-PEDOT:SSS: Black phosphorene-poly(3,4–ethylenedioxythiophene)–poly(styrenesulfonate), PC: porous carbon.

3.8. Real sample analysis

Furthermore, the practicability and reliability of the AuNPs@NSC-modified sensor are investigated by a commercially-available rutin capsule, in which medicinal rutin capsules of 10 mg/per capsule were examined as a standard sample. Ten capsules were opened, and the entire mass was diluted in 100 mL of a PBS buffer solution/ethanol (75:25 v/v) at pH 4. The binders, fillers and other ingredients were separated by filtration. The exact concentration of rutin in the obtained stock solution was examined using calibration curve technique. Table S2 summarizes the results of three parallel measurements that exhibited recoveries of 96.9%, 97.3%, and 97.5%, demonstrating that AuNPs@NSC is a good electrode material for the accurate and reliable determination of a real sample.

4. Conclusions

In summary, gold nanoparticles hosted by a nitrogen-doped silk carbon (AuNPs@NSC) composite were synthesized through *in situ* reduction and a subsequent carbonization protocol. Furthermore, a flexible three electrode sensor system with an AuNPs@NSC modified working electrode was developed and showed superb electrochemical activity for the analysis of rutin. The experimental results demonstrated a linear detection range of 0.11–250 μM for a rutin solution with 1.52% RSD, which could be attributed to the high content of nitrogen and good distribution of the AuNPs throughout the bulk. An applicability of the as-prepared sensor was verified using a commercially available product (Rutin capsule, 10 mg/capsule), and the sensor provided high precision with a minimum RE of 3.3%. The experimental results of the AuNPs@NSC-modified sensor offer a reliable approach and great opportunity in the field of electrocatalysis beyond the estimation of rutin.

Conflict of interest statement

We declare that we do not have any commercial or associative interest that represents a conflict of interest in connection with the work submitted.

Declaration of competing interest

The authors declare that they have no known competing financial interests or personal relationships that could have appeared to influence the work reported in this paper.

CRediT authorship contribution statement

Aniruddha Balkrishna Patil: Conceptualization, Methodology, Validation, Formal analysis, Investigation, Resources, Data curation, Writing - original draft, Visualization, Project administration. **Yafen Huang:** Formal analysis. **Liyun Ma:** Data curation, Writing - original draft. **Ronghui Wu:** Data curation, Writing - original draft. **Zhaohui Meng:** Formal analysis. **Lingqing Kong:** Data curation. **Wenli Zhang:** Formal analysis. **Qiang Liu:** Formal analysis. **Xiang Yang Liu:** Conceptualization, Methodology, Data curation, Writing - review & editing, Visualization, Supervision, Project administration, Funding acquisition.

Acknowledgment

This work was supported by the National Natural Science Foundation of China (Grant Nos. 51502253, U1405226, 21503175, and 21705135), Natural Science Foundation of Guangdong Province (Grant No. 2016A030310369), Natural Science Foundation of Fujian Province (Grant No. 2017J01104), the Fundamental Research Funds for the Central Universities of China (Grant Nos. 20720160127 and 20720180013), Doctoral Fund of the Ministry of Education (Grant No. 20130121110018), NUS AcRF Tier 1 (Grant No. R-144-000-367-112), the"111"Project (Grant No. B16029), and the 1000 Talents Program funding from the Xiamen University. The authors also thank the

technical supports from Li-Kun Yang, Hao Wang, Rui Yu Yun Yang, Dr. T. P. Ghule and Dr. Chhaya Panse (Principal M. D. College, Mumbai).

Appendix A. Supplementary data

Supplementary data to this article can be found online at https://doi.org/10.1016/j.bios.2019.111595.

References

Abdelhamid, H.N., Talib, A., Wu, H.-F., 2017. Talanta 166, 357–363.
Apetrei, I.M., Apetrei, C., 2018. Measurement 114, 37–43.
Freitas, K.H.G., Medeiros, R.A., Fatibello, O., 2009. Anal. Lett. 42 (6), 881–897.
Gaur, S., Miller, J.T., Stellwagen, D., Sanampudi, A., Kumar, C., Spivey, J.J., 2012. Phys. Chem. Chem. Phys. 14 (5), 1627–1634.
Gholivand, M.B., Mohammadi-Behzad, L., Hosseinkhani, H., 2016. Anal. Biochem. 493, 35–43.
Gullón, B., Lú-Chau, T.A., Moreira, M.T., Lema, J.M., Eibes, G., 2017. Trends Food Sci. Technol. 67, 220–235.
Hou, C., Xu, Z.J., Qiu, W., Wu, R.H., Wang, Y.N., Xu, Q.C., Liu, X.Y., Guo, W.X., 2019. Small 15 (11), 8.
Hou, J.H., Cao, C.B., Idrees, F., Ma, X.L., 2015. ACS Nano 9 (3), 2556–2564.
Hu, F., Liu, W.Z., Li, W.F., Xu, Z.J., Diao, Y.Y., Lin, N.B., Guo, W.X., Shi, L., van Esch, J.H., Liu, X.Y., 2019. Small 15 (13), 6.
Koh, L.D., Cheng, Y., Teng, C.P., Khin, Y.W., Loh, X.J., Tee, S.Y., Low, M., Ye, E.Y., Yu, H.D., Zhang, Y.W., Han, M.Y., 2015. Prog. Polym. Sci. 46, 86–110.
Liang, Y.-D., Song, J.-F., 2008. J. Electroanal. Chem. 624 (1), 27–32.
Lin, N.B., Cao, L.W., Huang, Q.L., Wang, C.Y., Wang, Y., Zhou, J., Liu, X.Y., 2016. Adv. Funct. Mater. 26 (48), 8885–8902.
Liu, Z., Xue, Q., Guo, Y., 2017. Biosens. Bioelectron. 89, 444–452.
Marti, R., Valcarcel, M., Herrero-Martinez, J.M., Cebolla-Cornejo, J., Rosello, S., 2017. Food Chem. 221, 439–446.
Niu, X., Wen, Z., Li, X., Zhao, W., Li, X., Huang, Y., Li, Q., Li, G., Sun, W., 2018a. Sens. Actuators B Chem. 255, 471–477.
Niu, X., Weng, W., Yin, C., Niu, Y., Li, G., Dong, R., Men, Y., Sun, W., 2018b. J. Electroanal. Chem. 811, 78–83.
Omenetto, F.G., Kaplan, D.L., 2010. Science 329 (5991), 528–531.
Omidfar, K., Khorsand, F., Azizi, M.D., 2013. Biosens. Bioelectron. 43, 336–347.
Petroski, J., Chou, M., Creutz, C., 2009. J. Organomet. Chem. 694 (7), 1138–1143.
Tao, H., Kaplan, D.L., Omenetto, F.G., 2012. Adv. Mater. 24 (21), 2824–2837.
Tu, H., Yu, R., Lin, Z.F., Zhang, L., Lin, N.B., Yu, W.D., Liu, X.Y., 2016. Adv. Funct. Mater. 26 (48), 9032–9043.
Wang, Q., Jian, M., Wang, C., Zhang, Y., 2017a. Adv. Funct. Mater. 27 (9), 1605657.
Wang, Y.H., Huang, K.J., Wu, X., 2017b. Biosens. Bioelectron. 97, 305–316.
Wu, Y., Hu, C.X., Huang, M., Song, N.N., Hu, W.B., 2015. Ionics 21 (5), 1427–1434.
Xie, J., Zheng, Y., Ying, J.Y., 2009. J. Am. Chem. Soc. 131 (3), 888–889.
Xu, H., Li, Y., Tang, H.W., Liu, C.M., Wu, Q.S., 2010. Anal. Lett. 43 (6), 893–904.
Yalikun, N., Mamat, X., Li, Y., Hu, X., Wang, P., Hu, G., 2019. Microchimica Acta 186 (6), 379.
Yang, B., Bin, D., Zhang, K., Du, Y., Majima, T., 2018. J. Colloid Interface Sci. 512, 446–454.
Yang, H., Li, B., Cui, R., Xing, R., Liu, S., 2017. J. Nanoparticle Res. 19 (10).
Yang, M., Zhou, Z., 2017. Adv. Sci. 4 (8), 10.
Yang, S.L., Qu, L.B., Li, G., Yang, R., Liu, C.C., 2010. J. Electroanal. Chem. 645 (2), 115–122.
Yildirim, S., Kadioglu, A., Saglam, A., Yasar, A., 2017. Instrum. Sci. Technol. 45 (1), 35–48.
Yu, H.L., He, Y., 2015. Sens. Actuators B Chem. 209, 877–882.
Zhan, T.R., Sun, X.Y., Wang, X.Z., Sun, W., Hou, W.G., 2010. Talanta 82 (5), 1853–1857.
Zhu, B., Wang, H., Leow, W.R., Cai, Y., Loh, X.J., Han, M.Y., Chen, X., 2016. Adv. Mater. 28 (22), 4250–4265.
Zhu, Y., Sun, W., Luo, J., Chen, W., Cao, T., Zheng, L., Dong, J., Zhang, J., Zhang, M., Han, Y., Chen, C., Peng, Q., Wang, D., Li, Y., 2018. Nat. Commun. 9 (1), 3861.
Zou, C.e., Bin, D., Yang, B., Zhang, K., Du, Y., 2016. RSC Adv. 6 (109), 107851–107858.